Field and Laboratory Validation of Photoactivated Adsorption for Removal of Arsenic in Groundwaters

State of Wisconsin Department of Natural Resources

Project No. 179 (NMD00000240)

Principal Investigator:

Marc A. Anderson
Professor
Environmental Chemistry & Technology Program
University of Wisconsin – Madison
660 North Park Street
Madison, WI 53706

Phone: 608-262-2674
Fax: 608-262-0454
E-mail: nanopor@wisc.edu

Start Date: July 1, 2003

End Date: June 30, 2004

FINAL REPORT

October 2004

Table of Contents

Field and Laboratory Validation of Photoactivated Adsorption for Removal of Arsenic in Groundwaters

Introduction

There is growing awareness of the chronic toxic effects of arsenic in drinking water. Because of these concerns, the U.S. Environmental Protection Agency (EPA) has lowered the maximum contaminant level (MCL) in drinking water from the present 50 ppb to 10 ppb, effective in 2006. This change is expected to have a particularly large impact on small communities that utilize ground water contaminated with arsenic as a source of drinking water [Frost et al, 2002]. Such communities have limited financial resources available to implement the additional treatment steps required to comply with the proposed change in the MCL for arsenic. As a result, EPA and other agencies have supported many studies directed at characterizing and developing alternative technologies for arsenic treatment that could be less expensive and more easily monitored than present commercially available approaches.

A primary reason for the expense associated with removing arsenic from water is that arsenic is generally present in two forms that behave differently. (Although additional forms of arsenic have been identified in water samples, the concentrations of these species of arsenic are low enough that they do not concern regulators.) Arsenate, As (V), is an oxyanion with the first two pK values reported as 2.66 and 6.77 [Smith and Martell, 1976], which indicates that As (V) exists as a charged anion over the pH range of 6 to 8.5 that is typical of drinking waters. Therefore, technologies such as adsorption, ion exchange, and coagulation/filtration are effective methods for treating arsenate. It appears that the treatment method used most commonly for removing As (V) is to adsorb it on activated alumina and dispose of the saturated adsorbent as a hazardous waste. This approach is favored because of its low capital costs and operating expenses [EPA, 2000]. However, the effectiveness of As (V) adsorption on activated alumina depends greatly on the pH of the system and on the concentrations of other species in the water being treated.

An additional problem arises in treating arsenite, As (III). Because the first pK for this species is 9.22 [Smith and Martell, 1976], most As (III) is uncharged in drinking water and much more difficult to remove than As (V). Present technologies first oxidize As (III) to As (V) and then treat the As (V), which requires at least one additional processing step. Arsenite is less of a concern in surface waters that contain some dissolved oxygen, which can slowly oxidize As (III) to As (V). However, As (III) can be the predominant form of arsenic in ground waters when they are first drawn from a well [Smedley and Kinniburgh, 2002; Johnson and Aldstadt, 2002].

The project discussed in this final report is based on earlier studies performed at the University of Wisconsin – Madison. These earlier studies involved two different treatment approaches. In one, a magnesium aluminate spinel was investigated as an alternative adsorbent for As (V). This spinel was observed to maintain its adsorption capacity for arsenate up to pH 7 as compared to γ-alumina (synthesized as a surrogate for activated alumina), which loses capacity at pH 6, a value that is typical of many activated aluminas [Rosenblum and Clifford, 1984; Clifford, 1999]. A second study involved the successful use of photocatalytic oxidation to convert As (III) to As (V) in synthetic laboratory solutions.

This project was proposed as a continuation of these earlier studies and incorporated five main tasks. **Task 1:** Characterize the adsorption chemistry of arsenic on a commercial activated

alumina, specifically focusing on the effect of competitive and cooperative adsorption (i.e., the effect of having other components present in the source water being treated) on the removal of arsenic. **Task 2:** Optimize the performance of a composite photocatalytic/adsorption medium containing two components, one a titania-based active photocatalyst to photooxidize As (III) to As (V) and the other an alumina-based adsorbent to remove photogenerated As (V) as it formed. **Task 3:** Develop methods to coat this composite on a near-UV transparent substrate for use in a waveguide photoreactor. (In a waveguide photoreactor, the activating light is carried through a transparent substrate and activates a coating of photocatalyst on the substrate whenever the light reflects off the substrate and the underside of the photocatalyst. This approach should illuminate the reactor and photocatalyst more uniformly than in a conventional photoreactor.) **Task 4:** Field test the waveguide photoreactor at a drinking water treatment plant in a small community with arsenic-contaminated water. **Task 5:** Develop a cost-benefit analysis for the performance of this system as compared to other commercial systems for arsenic treatment.

There were two reasons for performing Task 1. For one, it was felt that additional studies would clarify inconsistencies in reported results on the effect of pH on the adsorption density of arsenate onto activated alumina. In addition, one concern in evaluating the results of a field test would be accounting for the effect that the competitive and cooperative adsorption of other ions in the water being treated would have on the removal of arsenic. It has been shown that the presence of sulfate significantly lowers the adsorption density of arsenate on activated alumina [Clifford, 1999; Wang et al, 2000]. Although sulfate is not a concern at the test site of interest, it is present in many groundwaters and can reach concentrations of several hundred ppm [WHO, 2003 draft]. Adsorption studies for this task focused on systems that contained both sulfate and arsenate. Additional studies were performed with silicate, which is present in the ground water at the test site. The effect of adding magnesium was monitored because it had been shown to enhance arsenate adsorption in earlier laboratory studies and is present in hard water.

By the start of this project, it was apparent that laboratory tests involving Task 2 should be directed towards three specific sub-objectives to further elucidate the behavior of the system during the photocatalytic oxidation of arsenite. **A)** Determine the effect of the concentration of dissolved oxygen on the rate of photooxidation of As (III). **B)** Determine if the As (V) formed by the photooxidation of As (III) was adsorbed on the photocatalyst and, if so, whether or not this adsorption decreased the rate of photooxidation of As (III). **C)** Compare the rates of photo-oxidation of As (III) in a synthetic laboratory water and in water obtained from the test site of interest to determine if the rate of photooxidation was affected by the presence of other species in an actual ground water. All tests involving Task 2 were performed with pure titania photocatalyst rather than the composite material in order to avoid confounding effects from the presence of an alumina-based adsorbent in the test system.

Task 3 was included in this project because of the realization that commercial acceptance of this technology required the development of a method for depositing the active materials on a substrate that could be readily scaled up for industrial use. Spray coating was investigated for this application using a system from Sono-Tek Corp. (Milton, NY).

Field tests for Task 4 were conducted at Danvers, IL, a small community about 10 miles west of Bloomington, IL, with the assistance of Thomas Holm, Ph.D., of the Illinois State Water Survey (ISWS). This site was chosen because members of the ISWS have a good understanding of its groundwater chemistry from previous studies they have conducted there. In addition, the manager of the drinking water treatment facility in Danvers was quite cooperative as the field tests were conducted in April and June of 2004. Because of time and resource constraints,

however, the first goal of the field tests was limited to determining if a small portable waveguide photoreactor could be used to photooxidize As (III) to As (V) in a field setting. If photooxidation was observed, as was expected based on the results of Task 2, then the second goal of these tests was to develop a kinetic expression for the photooxidation of As (III) that could eventually be utilized to design a scaled-up photoreactor for possible commercial use. This expression would also prove useful in performing the desired cost-benefit analysis for Task 5.

Although it was known from the results of Task 2 that the photocatalyst itself was able to adsorb some As (V), the amount of As (V) generated during a field test swamped the adsorption capacity of the photocatalyst present in the photoreactor. Available resources did not allow the inclusion of a separate adsorption column to remove photogenerated As (V). In addition, the photoreactor employed for this study had been designed for use with a special light source that could not be used safely in a field test. As a result, the photoreactor was not well-matched with the light source that was employed. Given these concerns, the cost-benefit analysis proposed for Task 5 was not performed because it was felt that the results would have little applicability.

Results of these tasks are presented in the following three chapters of this final report. Studies performed for Tasks 1 and 2 are presented in Chapters 1 and 2, respectively. Results for Tasks 3 and 4 are combined in Chapter 3 because spray coating was utilized to prepare the waveguide photocatalyst incorporated in the photoreactor used for the field tests. Conclusions and recommendations resulting from this project are given in the final section. Note that, as a result of an incompatibility between the versions of Sigma Plot and Microsoft Word used to prepare this report, the y-axis label for the graphs shown in Chapters 1 and 2 is not displayed. The label is given in the figure captions for the affected figures.

Chapter 1

Effect of Competitive Adsorption of Other Species on Arsenate Uptake on Activated Alumina

Introduction

Adsorption processes are commonly employed to treat arsenic in drinking water systems because of the relatively low capital costs and low operating expenses associated with these processes [Chen et al, 1999]. Because of its low cost and high surface area, activated alumina, which is available in many forms, has been the preferred adsorbent. Rosenblum and Clifford [1984] found that the adsorption capacity of activated alumina decreases significantly when the pH increases above 5.7, with the adsorption capacity being 14 times higher at pH 6.0 than at pH 7.5 [Clifford, 1999].

Adsorption on hydrous oxides such as activated alumina should be pH dependent [Clifford, 1999] because such materials are amphoteric, i.e., they display both acidic and basic properties depending on the pH of the system. One way of estimating the degree of acidity or alkalinity of the material is by measuring its zeta potential (electrokinetic potential at the slipping plane of the particle – the region around the particle inside of which the solvent and associated ions move with the particle under the influence of an external electric field) as a function of pH. The isoelectric point (IEP) is defined as the pH at which the zeta potential of the colloidal particle (the adsorbent in this case) is zero [Lyklema, 1983]. Therefore, the particle should be neutral at that pH because its positive and negative surface charges should balance. Decreasing the pH causes the particle to become positively charged, whereas increasing the pH causes a negative charge to develop.

Since the IEPs of many activated aluminas are around 8.2, they should adsorb negatively charged arsenate quite well when the pH of the source water is lower than 8.2. However, previous studies have shown that the optimal pH range for adsorbing As (V) on activated alumina is 5.5 – 6.0, which is much lower than its IEP [Hathaway and Rubel, 1987; Clifford, 1999]. The reason for this discrepancy is that the chemical adsorption of anions such as arsenate (and other oxyanions such as phosphate) increases the negative charge on the adsorbent and decreases its IEP [Anderson, 1974]. The magnitude of this shift increases as the concentration of the adsorbing anion increases until the maximum amount of the anion is adsorbed. Therefore, the IEP of the adsorbent depends on the concentration of adsorbates in contact with the adsorbent.

Anion competition is a significant factor that can contribute to a reduced capacity for adsorbing arsenate. For instance, the presence of sulfate decreases the adsorption capacity of adsorbents for arsenate [Clifford, 1999]. Generally, As (V) has a higher affinity for the adsorption sites on activated alumina than most other anions with the possible exception of phosphate [Clifford, 1999]. However, the concentrations of anions in ground water (at pH values greater than 8.5) are often between 10 to 10,000 times that of arsenate [Holm, 2002]. It is certainly conceivable that anions present at these elevated concentrations, even if they are less strongly bound, may compete with arsenate for sorption sites. The reverse process (i.e., cooperative adsorption) can occur for cation adsorption, although the effect is less dramatic because most cations do not appear to bond chemically to oxides. In addition, adsorption of uncharged species on adsorbents could affect the amount of arsenate that can be removed.

Commercial applications of this technology for treating contaminated waters require experience in dealing with the effects of other chemical species on the removal of arsenate on the oxide-based adsorbents used in this study. A commercial activated alumina was chosen as the adsorbent for study to gain familiarity with the behavior of a commercial product. Most of the studies were directed at determining the effects of sulfate on the removal of arsenate because sulfate can be found at relatively high concentrations in groundwaters [WHO, 2003 draft]. Typical concentrations range from 0 to 250 mg/L (2.6 mM) [WHO, 2003 draft]. Although sulfate was not present in the water at the test site of interest, magnesium (ca. 30 ppm) and silica (7.5 ppm) were present. Additional tests were conducted to determine the effects of adding these species on the adsorption of arsenate.

Procedures

All solutions for this study were prepared using ultra-pure water obtained from a Barnstead (Dubuque, IA) NANOpure UV purification system. All testing equipment was cleaned by soaking in 10% HCl for more than eight hours and rinsing four times with ultra-pure water. The arsenate stock solution (1000 μg As/L) was prepared from solid sodium arsenate, $Na_2AsO_4 \cdot 7H_2O$, (Aldrich, ACS primary standard) dissolved in 0.01 M $NaNO_3$ (Sigma, ACS primary standard) to buffer effects from changes in ionic strength. Activated alumina (AA-400G with a specific surface area of 320 m^2/g) was provided by Alcan Chemical Inc. (Chicago, IL). Batch experiments were conducted to study the uptake of arsenate on this activated alumina with and without competition from other species. These tests utilized a fixed initial concentration of sulfate, silicate, or magnesium and ca. 0.2 g of activated alumina, but each sample was adjusted to different initial pH values using 0.01 M $NaNO_3$ as a background electrolyte. During this study, zeta potential changes were monitored using a Malvern Instruments (Southborough, MA) Zetasizer 3000.

Each test was started by adding 50 mL of the desired test solution (i.e., adsorbent concentration is 4 g/L) to a 50-mL polypropylene centrifuge tube (Becton, Dickinson and Co., Franklin Lakes, NJ) and adjusting the pH of the test solution with 0.1 M NaOH and 0.1 M HNO_3 to cover the pH range from 4.5 to 11.0. For tests involving sulfate, after addition of one or both anions simultaneously, suspensions were shaken for seven days and pH was adjusted daily. Initial concentrations of arsenate were either 0 mM or 0.5 mM (37.5 ppm As) and initial concentrations of sulfate were 0, 1.0 (32 ppm S), and 2.5 mM (80 ppm S), which is typical of sulfate concentrations in groundwater. (The high concentration of arsenate was employed in order to obtain observable shifts in zeta potential. Such shifts would not be seen at typical environmental concentrations of arsenate.) Concentrations of both arsenate and sulfate were determined using inductively coupled plasma – atomic emission spectroscopy (ICP-AES). Anion adsorption was calculated from the difference in total anion and equilibrium solution anion concentrations. A similar approach was employed for experiments involving silicate (0.7 mM or ca. 20 ppm Si) and magnesium (2.5 mM or 60 ppm Mg).

At the conclusion of the 1-week equilibration and pH adjustment period, the final pH of each sample was measured 3 min after immersing the pH electrode in the solution. Zeta potential was then measured using 20 mL of each sample. The remaining 30 mL was filtered with a 0.45 μm membrane filter (Millipore, Billerica, MA) with the first 15 mL wasted and the remaining 15 mL samples analyzed by ICP. Initial concentrations of arsenic and the other species of interest were determined using a control sample containing the same initial concentrations of arsenate and the other species as the test samples but without activated alumina. Approximately 30 mL of

the control sample was filtered as described above. The remaining 20 mL was not filtered. No significant differences in concentrations were found between filtered and non-filtered samples.

The instrument employed for the ICP measurements was a Perkin Elmer (Norwalk, CT) Optima 4300 operated at 188.975 nm for arsenic, 386.015 nm for sulfur, 251.611 nm for silicon, and 279.535 nm for magnesium. Perkin Elmer reports detection limits of 5, 10, 12, and 0.2 µg/L for each of these elements, respectively. Certified ICP standard solutions containing 1000 mg As/L (Spex Certi Prep. Inc., Metuchen, NJ), 1000 mg S/L (Ricca Chemical Inc., Chicago, IL), 10,300 mg Si/L (Aldrich Chemical, St. Louis, MO), and 1,000 mg Mg/L (EM Science, Inc., Hawthorne, NY) were used to prepare all calibration solutions.

Latex standards (supplied by Malvern) were used to verify performance of the Zetasizer 3000. Zeta potential standards with an accepted value of -50 mV were injected before measurements and a ±10% error margin was accepted. All zeta potentials were measured for suspensions containing activated alumina using a 0.01 M $NaNO_3$ background electrolyte to minimize the effect of changes in the ionic strength of the suspensions.

Results and Discussion

Effect of Sulfate: Figure 1.1 compares the zeta potential of the activated alumina in the background electrolyte only and in contact with 2.5 mM sulfate. The IEP of this activated alumina in the absence of sulfate was 8.1, which agrees with previous research [Clifford, 1999]. Its IEP was not significantly lowered in the presence of sulfate, although the zeta potential values were significantly less positive at pH values below the IEP. This result supports the belief that sulfate does not bond chemically to activated alumina [He et al, 1997; Goldberg and Johnston, 2001] or to other oxides [Hansmann and Anderson, 1985]. The decrease in zeta potential below the IEP indicates that sulfate ions are present inside the slipping plane of the particles and are held by electrostatic attraction and/or hydrogen bonding to the positively charged particles.

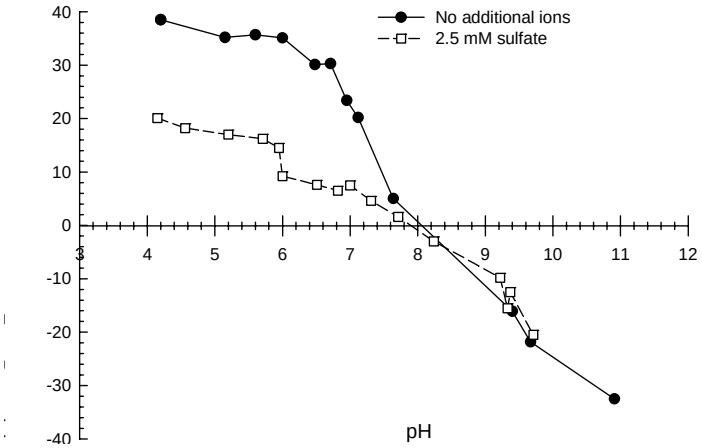

Figure 1.1 Effect of sulfate adsorption on zeta potential, which is shown in mV as the y axis of this figure. Samples consisted of 0.2 g of activated alumina (AA-400 G, Alcan) in 50 mL of solution with and without sulfate using 10 mM $NaNO_3$ as background electrolyte.

As shown in Figure 1.2, the IEP of activated alumina decreased to 7.5 from 8.1 in the presence of 0.5 mM arsenate. Such shifts in the IEPs of minerals with increasing ion concentration generally indicate that the ion has chemically bound to the adsorbent [Goldberg and Johnston, 2001]. Even though the presence of sulfate alone did not alter the IEP of activated

alumina, the results in Figure 1.2 suggest the synergistic effect of the presence of both sulfate and arsenate on the IEP, which decreased to 6.5 when in contact with 0.5 mM arsenate and 2.5 mM sulfate. This change could indicate that the presence of sulfate causes more arsenate to adsorb on the activated alumina or that the chemical adsorption of arsenate somehow leads to the co-adsorption of sulfate on the surface of the activated alumina.

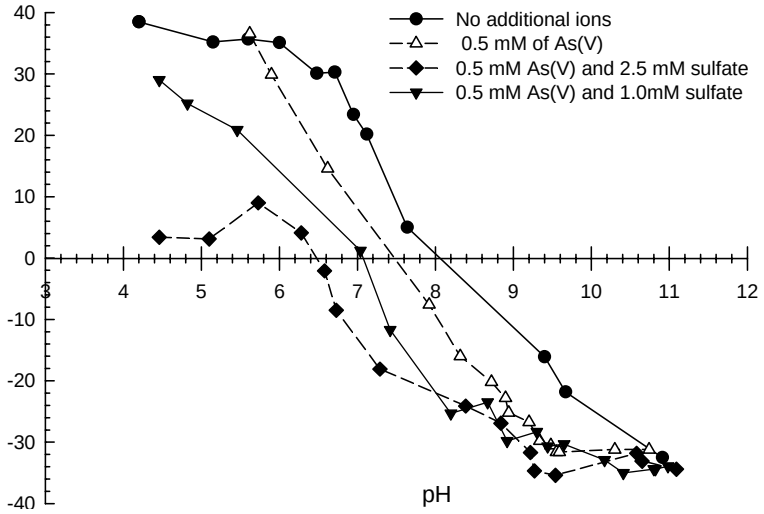

Figure 1.2 Effect of anion adsorption on zeta potential, which is shown in mV as the y axis of this figure. Samples consisted of 0.2 g of activated alumina (AA-400 G, Alcan) in 50 mL of solution with and without anion species in 10 mM $NaNO_3$ as background electrolyte.

Further data was obtained from the adsorption studies performed on activated alumina. Figure 1.3 shows that the adsorption density of 2.5 mM sulfate on activated alumina was reduced significantly over the entire pH range by adding 0.5 mM arsenate. This observation is reasonable because the adsorption of arsenate makes the surface of the activated alumina more negative at pH values above ca. 6.0 and a more negative surface decreases the adsorption of sulfate by electrostatic repulsion. (As shown in Figure 1.2, the addition of arsenate and sulfate decreased the IEP of the system from 8.1 to 6.5.) In addition, this observation contradicts the second explanation given above for the behavior observed in Figure 1.2. Regardless of whether or not arsenate was present, only a negligible amount of sulfate was adsorbed on the activated alumina at pH values above the IEP, as previously reported [Geelhoed et al, 1997], which supports the idea that sulfate adsorption is driven primarily by electrostatic attraction.

In contrast, as shown in Figure 1.4, the addition of 2.5 mM sulfate reduced the adsorption density of 0.5 mM arsenate over a fairly narrow pH range (from 6.5 to 9.5), with no detectable reduction in arsenate adsorption when the pH was less than 6.5. For these systems, the addition of sulfate reduces the IEP from 7.5 to 6.5, which makes the activated alumina more negative in this pH range and thus appears to inhibit the adsorption of arsenate to some extent. In addition, though, this observation contradicts the first explanation given above for the behavior observed in Figure 1.2. At present, we do not understand the reason(s) underlying the behavior shown in this figure. It may indicate that surface speciation and surface protonation reactions are occurring that could only be elucidated by further studies using surface spectroscopy techniques. Finally, although the adsorption of arsenate decreases noticeably at pH values above the IEP in both

systems, there is measurable adsorption of arsenate at pH values that are as much as 4 units above the IEP. This behavior can occur when an adsorbate chemically bonds to the adsorbent.

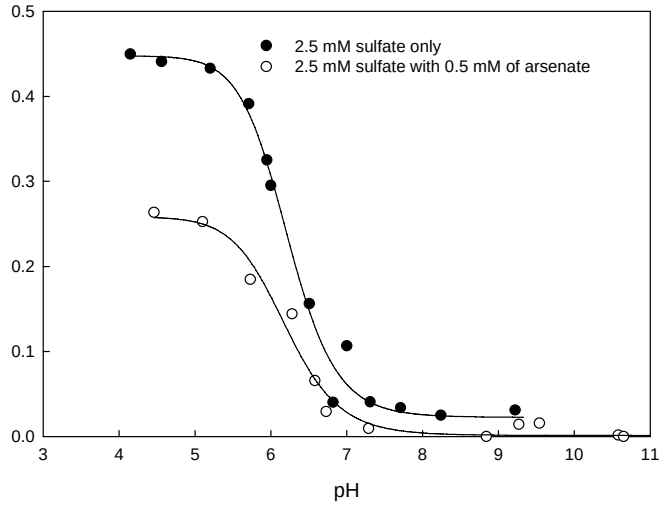

Figure 1.3. Sulfate adsorption on activated alumina (4 g/L) with and without arsenate in 10 mM $NaNO_3$ as background electrolyte. The y axis represents the adsorption density in mmol/g.

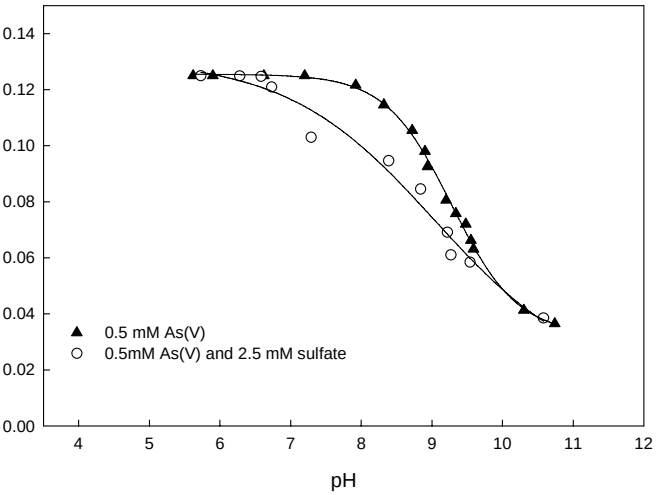

Figure 1.4. Arsenate adsorption on activated alumina (4 g/L) with and without sulfate in 10 mM $NaNO_3$ as background electrolyte. The y axis represents the adsorption density in mmol/g.

Effect of Silicate: Figure 1.5 shows the effect of silicate (0.7 mM) and arsenate (0.5 mM) on the IEP of activated alumina. In contrast to the behavior observed when sulfate was added to a suspension of activated alumina (no shift in IEP), the addition of silicate decreased the IEP of the activated alumina from 8.1 to 6.6. This decrease indicates that the added silicate is chemically binding to the activated alumina in some manner or possibly precipitating on the activated alumina. This interaction does not involve electrostatic attraction because the first pK for silicic acid is ca. 9.5, so silicate is uncharged over most of this pH range. The presence of arsenate in this system results in further chemical bonding to the adsorbent and a further decrease in IEP to 4.8.

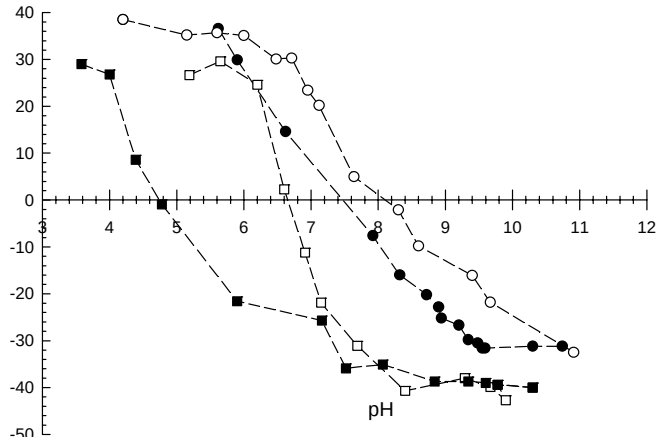

Figure 1.5 Effect of anion adsorption on zeta potential, which is shown in mV as the y axis of this figure. Samples consisted of 0.2 g of activated alumina (AA-400 G, Alcan) in 50 mL of solution that contained 10 mM $NaNO_3$ as background electrolyte. (o) No additional ions; (●) 0.5 mM As (V); (□) 0.7 mM silicate; (■) 0.5 mM As (V) and 0.7 mM silicate.

One result of the adsorption of silicate is that the surface of the adsorbent becomes more silica-like. Zhuang and Yu [2002] have suggested that a thin layer of an aluminosilicate mineral might form on this surface. Most forms of silica and aluminosilicates have IEP values in the range of 2 to 3. Therefore, these surfaces will have a large negative charge in natural waters and would be expected to adsorb only limited amounts of arsenate.

This expectation is supported by the data shown in Figure 1.6 A and B. Figure 1.6A indicates that adding 0.7 mM (20 ppm) silicate to the test system decreases the adsorption density of arsenate considerably over the pH range tested. Although some of this decrease probably results from the deposition of some form of silica on part of the adsorbent, part of the decrease results simply from the drop in the IEP of the adsorbent (from 8.1 to 4.8) that occurs in the presence of these adsorbates. Figure 1.6B shows that the amount of silicate adsorbed increases somewhat with increasing pH, as reported by Xiao and Lasaga [1994] and Meng et al. [2000], but is relatively independent of the amount of arsenate present in the system. Even though arsenate binds chemically to the activated alumina, this binding does not appear to affect the deposition of silicate on the activated alumina.

These results suggest the possibility that natural waters containing even higher levels of silicate than employed for this test might deposit enough silica on the adsorbent to eliminate its ability to remove adsorbates such as arsenate at any pH. Further tests would be required to verify this hypothesis. Even at the silicate concentrations employed for these tests, it is clear that the presence of silicate in the water being treated will both lower the adsorption density of arsenate at a given pH and lessen the effect of pH changes on the adsorption density of arsenate.

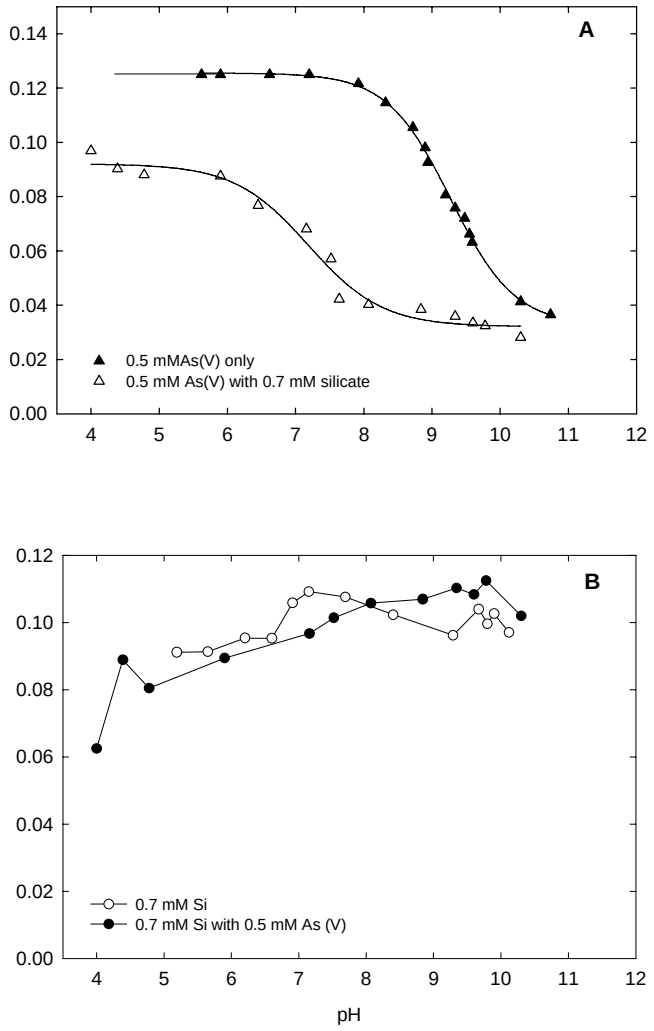

Figure 1.6. A) Arsenate adsorption on activated alumina (4 g/L) with and without silicate in 10 mM $NaNO_3$ as background electrolyte. B) Silicate adsorption on activated alumina (4 g/L) with and without arsenate in 10 mM $NaNO_3$ as background electrolyte. The y axis represents the adsorption density in mmol/g in both figures.

Effect of Magnesium: The addition of 2.5 mM magnesium nitrate (60 ppm Mg) to 0.2 g of activated alumina suspended in 50 mL of 0.01 M sodium nitrate increased the IEP of the activated alumina from 8.1 to 10.5. Further addition of 0.5 mM arsenate (37.5 ppm As) lowered the IEP to 8.5, about 1 pH unit higher than the IEP obtained when 0.5 mM arsenate adsorbs on the activated alumina with no magnesium present. In the system containing magnesium and arsenate, the amount of arsenic remaining in solution is near zero at all pH values up to ca. 11. One factor affecting the adsorption of arsenate in this system is that equilibrium calculations indicate that brucite, $Mg(OH)_2$, may start to precipitate above pH 8.5 under these conditions. This phenomenon has been reported previously (Sun and Gao, 2002). Calcium present in the groundwater would be expected to behave similarly to magnesium, which suggests that it may be easier to remove arsenate from groundwaters before these waters have been softened.

Tests with Actual Groundwaters: Tests were also conducted using groundwaters obtained from Madison, WI and Danvers, IL after passing these waters through a 0.45 μm membrane filter. The Madison groundwater contained ca. 25 ppm Mg, 50 ppm Ca, no detectable iron, 5 ppm Si, 25 ppm sulfate, and < 1.5 ppm organic matter. The IEP of activated alumina in this water was ca. 9.3. This rather high value is most likely caused by the hardness of the water. When 0.5 mM arsenate is also present, the IEP decreases to ca. 8.2. Almost all the arsenate is adsorbed when the pH of this water sample is less than 7, and ca. 90% is removed at pH 8. As expected, the removal of arsenic was much less effective at pH values above the IEP of 8.2, although roughly 30% of the arsenic was still adsorbed at pH 10.

The behavior using the Danvers water was different. This water contained ca. 30 ppm Mg, 70 ppm Ca, 3 ppm iron, 7.5 ppm Si, no detectable sulfate, and ca. 13 ppm organic matter. The zeta potential of activated alumina in this water was negative at all pH values tested (pH 4.5 to 10.5). Although some adsorption of added arsenate was observed, it was only ca. 60% of the arsenate at the lowest pH. Although this water is harder than the Madison water, the presence of higher levels of silica and particularly organic matter caused a significant decrease in the performance of this activated alumina. The effect of organic matter in this system is not surprising once it is realized that the carboxyl and phenol groups that are plentiful in this material can cause it to be negatively charged at pH values as low as 4 (Holm 2003). Adsorbents exposed to water containing humic acid, often a major component of dissolved organic matter, have been shown to adsorb considerably less arsenate than when humic acid is not present (Dousova et al, 2003; Cornu et al, 2003).

Conclusions

1. In many cases, adsorption densities of arsenate onto activated alumina correlate with the IEP of the activated alumina. Maximum adsorption occurs at pH values less than the IEP, with the adsorption density remaining relatively constant. Arsenate adsorption decreases dramatically at pH values greater than the IEP. However, the location of the IEP of activated alumina varies depending on the types and concentrations of the other species present in the treatment water.
2. Silicate appears to chemically bind to activated alumina. As a result, adsorption densities for silicate on activated alumina do not correlate well with IEP. Silicate adsorption decreases the IEP of activated alumina.
3. Silicate competes with arsenate for adsorption sites on activated alumina. Therefore, in the presence of silicate, the adsorption density of arsenate is decreased for pH values less than the IEP of the activated alumina (with adsorbed silicate). The adsorption density of arsenate is not greatly affected by silicate when the pH is greater than the IEP.
4. Sulfate does not appear to chemically adsorb on activated alumina and so does not compete directly with arsenate for adsorption sites. As a result, the addition of only sulfate does not change the IEP of activated alumina. However, when both sulfate and arsenate are present, the IEP of activated alumina decreases considerably more than if only arsenate is present. Whether or not sulfate is present, the adsorption density of arsenate remains relatively constant at pH values less than the IEP of activated alumina. At pH values greater than the IEP, arsenate adsorption decreases dramatically.
5. The presence of magnesium increases the IEP of activated alumina. Although the adsorption density for arsenate is similar in the presence or absence of magnesium,

adding magnesium to the treatment water increases the pH range over which activated alumina is effective at removing arsenate.

6. Even though activated alumina is considered to be effective at removing arsenate because activated alumina is a positively charged adsorbent, the surface charge of activated alumina can be negative in certain water matrices (e.g., water from Danvers, IL that contains a variety of dissolved species). This change in surface charge may be caused by the presence of high concentrations of organic matter and silica. In cases like this, removal of arsenate can only occur by chemisorption; therefore, pH may not be a significant factor affecting arsenate adsorption.

Chapter 2

TiO_2-Mediated Photocatalytic Oxidation of Arsenite to Arsenate

Introduction

Arsenate, As (V), can be removed from drinking waters by adsorption processes under appropriate operating conditions, which may require the acidification of the water being treated. Because arsenite, As (III), is uncharged at pH values typical of drinking water, this form of arsenic is much more difficult to remove. As (III) is typically removed by first oxidizing it to As (V) and then removing the arsenate using adsorption, precipitation, or ion exchange processes. Some of the processes being developed for arsenite oxidation include chemical and solid phase oxidants [Amy, 2000; Ghyrie and Clifford, 2001].

In a relatively recent patent, Khoe et al. [1997] claimed that photo-assisted oxidation using UV light effectively oxidizes As(III) to As(V). However, a pilot study conducted with a 200 nm UV light found that UV oxidation was only effective at extremely high UV intensities (7000 times the UV dose required for E. Coli inactivation) [Ghyrie and Clifford, 2001]. Even though Khoe et al. claimed that UV oxidation is effective at higher wavelengths (> 300 nm), Bissen et al. [2001] reported that only 54% of As(III) was oxidized in 45 minutes.

Recently, TiO_2-catalyzed photooxidation of As(III) to As(V) has been studied [Bissen et al, 2001; Lee and Choi, 2002]. UV oxidation occurs when the energy from the UV light source is transferred directly to the reaction. In contrast, TiO_2 photooxidation utilizes a semiconducting photocatalyst in a process that has been shown to effectively remove organic contaminants in water systems [Hoffmann et al, 1995]. In this process, the photocatalytic TiO_2 absorbs light that has energy greater than the band gap energy of the TiO_2 (about 3.2 eV or 380 nm light), producing electrons and holes on the surface of the oxide. The strongly oxidizing holes break down organic contaminants and can also convert As(III) to As(V). Lee and Choi [2002] observed that photooxidation by suspensions of TiO_2 effectively oxidizes As(III) to As(V). Bissen et al [2001] demonstrated that nanoparticulate suspensions of TiO_2 illuminated with UV light can oxidize As(III) to As(V) in less than three minutes, although it can be difficult to separate the treated solution and the particulate TiO_2 photocatalyst [Lee and Choi, 2002]. An alternative approach is to immobilize the TiO_2 by coating it on a substrate. However, only limited work has been done to verify the feasibility of this technology.

This aspect of the project was directed towards fulfilling three objectives. **A)** Determine the effect of the concentration of dissolved oxygen on the rate of photooxidation of As (III). **B)** Determine if the As (V) formed by the photooxidation of As (III) was adsorbed on the photocatalyst and, if so, whether or not this adsorption decreased the rate of photooxidation of As (III). **C)** Compare the rates of photooxidation of As (III) in a synthetic laboratory water and in water obtained from the test site of interest to determine if the rate of photooxidation was affected by the presence of other species in an actual ground water. All of these tests were performed with pure titania photocatalyst rather than the composite material that had been developed in earlier projects in order to avoid confounding effects from the presence of an alumina-based adsorbent in the test system.

Procedures

Materials: The titania photocatalyst was prepared by the following method. While 5,000 mL of 0.1 N nitric acid was stirred, 417 mL of titanium isopropoxide was added slowly, forming a cloudy white suspension. This suspension was continuously stirred for 3-4 days to peptize (i.e., break up) the suspension, resulting in the formation of a slightly cloudy, bluish sol. In order to increase the porosity of the final coating, the sol was dialyzed after peptization against ultra-pure water using a 1:10 volume ratio of sol to ultra-pure water. The water was changed daily for 3-4 days until a final pH of 3.5 was reached. The particle size in the dialyzed titania sol is in the range of 7 to 8 nm.

Once the titania sol was prepared, it was used to coat borosilicate glass Raschig rings. Before coating, the rings were calcined at 550°C to remove the organic matter on the surface, after which the rings were base treated by dipping into 0.1 M NaOH for more than 8 hours and rinsing with ultra-pure water. All rings were dip coated three times with the sol. For each coating, the rings were withdrawn from the sol and allowed to air dry under ambient conditions. After air drying, the coated rings were calcined at 350°C for three hours to form the nanoporous thin-film coating.

The average weight of each uncoated glass ring was 0.16 ± 0.01 g. A previous study found that the amount of coated TiO_2 deposited on each glass ring prepared using this technique was 0.305 ± 0.03 mg. Specific surface areas of the coated titanium dioxide were found to be 0.4 m^2 per gram of titania-coated glass rings [Sirisuk, 2003].

Analytical Methods: Concentrations of arsenic were determined by inductively coupled plasma – atomic emission spectroscopy (ICP-AES) using a Perkin Elmer (Norwalk, CT) Optima 4300 operated at 188.975 nm for arsenic. At this wavelength, Perkin Elmer reports detection limits of 5 μg/L. A certified ICP standard solution containing 1000 mg As/L (Spex Certi Prep. Inc., Metuchen, NJ) was used to prepare all calibration solutions. Arsenic speciation was accomplished by using Strong Anion Exchange cartridges (SAX, 3 mL, Supelco, Bellefonte, PA) to separate As(V) from arsenic solutions. A MasterFlex Pump (Cole-Parmer, Chicago, IL) was used to pass 5 to 6 mL of sampled solution through the cartridge at a flow rate of ca. 1.5-2.0 mL/min. Filtered samples contained As (III) while unfiltered samples contained total arsenic.

The level of dissolved oxygen (DO) was controlled by purging with nitrogen gas or compressed air (<0.1 ppm hydrocarbon). The gas pressure was adjusted to achieve desired DO concentrations. The DO level was measured using a YSI Model 58 DO meter (YSI, Yellow Springs, OH).

Test Solutions: All solutions for this study were prepared using ultra-pure water obtained from a Barnstead (Dubuque, IA) NANOpure UV purification system. All glassware was cleaned by soaking in 10% HCl and rinsing several times with deionized water. A 0.1 N sodium arsenite standard solution, $NaAsO_2$ (Alfa Aesar), was used as a stock solution. Note that this standard solution was determined to be equivalent to 0.0434 M arsenite, rather than the expected value of 0.1 M. All solutions, other than a sample of groundwater obtained from Danvers, IL, were prepared in 0.01 M $NaNO_3$ to provide a background matrix similar to that employed for the adsorption tests discussed in Chapter 1.

Test Configurations: A Pyrex® glass column (220 mm length × 170 mm diameter) was used to hold 19 g of glass rings that had been coated with photocatalyst. The estimated surface area of the photocatalyst was 7.6 m^2. The empty bed volume of the column when packed with rings was ca. 50 mL. Four Sylvania fluorescent bulbs (F15T8/350BL, 15 watt each) were used to illuminate the column containing the coated rings. Although this geometry does not provide

uniform illumination of the photoreactor, several readings of the light irradiance taken at different places were averaged to obtain an irradiance of 5 mW/cm^2 at the surface of the reactor. Irradiance measurements were obtained using an International Light Inc. (Newburyport, MA) Model IL 1400A radiometer/ photometer coupled to a Super Slim probe.

This reactor was used in two configurations: either for single-pass measurements (as shown in Figure 2.1A) or as a differential column batch reactor in which the test solution was recirculated through the reactor (as shown in Figure 2.1B). An initial single-pass study was conducted to obtain a general idea of the performance of the system. After the initial study, the system was reconfigured to allow recirculation. The recirculating system was employed for all tests conducted to fulfill the three objectives listed for this part of the project.

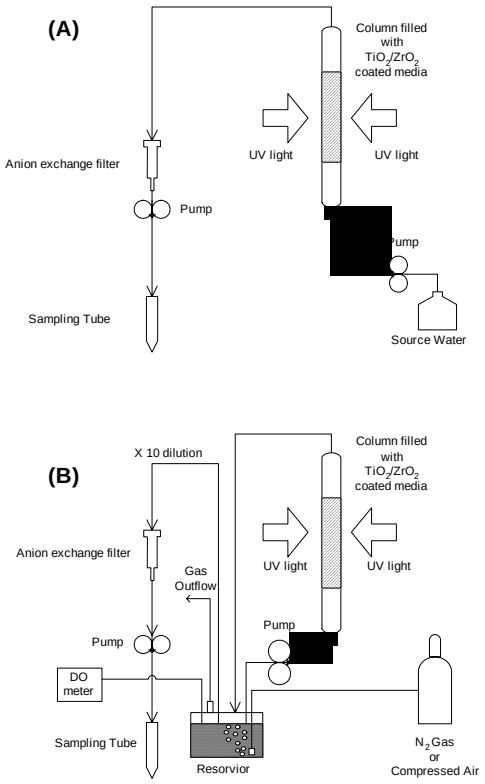

Figure 2.1. Schematic diagrams of (A) the single-pass test configuration and (B) the recirculating test configuration.

Testing Procedure: After adjusting the pH and the desired initial concentration of arsenic in the reservoir (1 L), the test solution was pumped into the prepared column at the desired rate. In the single-pass configuration, the flow rate was 5 mL/min, giving a 10-minute empty bed contact time (EBCT), and the treated solution was either sampled or sent to a collection vessel for disposal. For the recirculating configuration, a flow rate of 10 mL/min was employed (EBCT = 5 minutes), and the treated solution was recirculated back to the reservoir.

Sampling was performed periodically by either taking 1 mL of sample directly from the line or sampling from the reservoir. In either case, the 1-mL sample was diluted with 10 mL of ultra-pure water. About 6 mL of the diluted sample was filtered through the SAX cartridge to

remove As(V) and thus to determine the concentration of As(III), while the other 5 mL of diluted sample was analyzed to determine the total arsenic concentration.

Data Reduction: Data for the conversion of As (III) to As (V) obtained in all tests that employed the recirculating configuration were analyzed using a half-order model of reaction kinetics. Calculated reaction rate constants were then used to compare the performance of the system under different reaction conditions. This model was chosen because it had been shown to be effective in earlier studies of the photocatalytic oxidation of species in the gas phase [Zorn et al, 2000]. In this model, the rate of change of As (III) to As (V) is assumed to be proportional to the square root of the concentration of As (III) remaining in the test solution at a given time. As a result, the change in the concentration of As (III) as a function of time should obey the following equation:

$$(C/C_0)^{1/2} = 1 - k_{app}t$$

where: C = concentration of As (III) in a sample obtained at time t;
C_0 = concentration of As (III) at time t = 0, (i.e., the start of the test);
k_{app} = apparent rate constant for the reaction under study;
t = time after the start of the test at which the sample was obtained.

The apparent rate constant shown in this expression incorporates several terms that should be constant for the series of tests being compared, including the initial concentration of As (III) and the irradiance (i.e., light intensity) in the reactor. If k_{app} is constant, then a plot of $(C/C_0)^{1/2}$ against time should be linear. For the majority of the data sets obtained, r^2 values for the fit were greater than 0.98. The worst fit was obtained in a test involving an actual groundwater sample from Danvers, IL for which $r^2 = 0.934$. Note that a first-order model of reaction kinetics is used to analyze the kinetic data in many studies of photocatalytic oxidation in aqueous systems. For comparative purposes, however, the model employed to analyze the data simply has to fit the data reasonably well, which this model appears to do.

Simulating the Effect of Carbon in a Natural Water: After testing a groundwater sample from Danvers, efforts were made to duplicate some of those results using test solutions prepared with ultra-pure water and specific additives. To simulate the effect of inorganic carbon (H_2CO_3, HCO_3^-, CO_3^{2-}), 10 mM of sodium carbonate (120 mg/L as inorganic carbon) was added to a 2 mg/L As(III) solution. The pH of the solution was then adjusted to pH 7.0 with 0.1 M HNO_3 and NaOH before testing. Similar tests were performed in the presence of organic carbon by preparing a solution that contained 1 mM glucose ($C_6H_{12}O_6$) and 2 ppm As(III).

Results and Discussion

Single-Pass Configuration: Results of a single-pass column test in which the column was illuminated with near-UV light for 860 minutes are shown in Figure 2.2. The test solution, which consisted of 0.01 M $NaNO_3$ containing ca. 100 μg/L of As(III), was passed through the bed at a flow rate of 5 mL/min (EBCT = 10 min). At the start of this test, the concentrations of both total arsenic and As(III) in the outflow were around 20 μg/L, indicating that ca. 80% of As(III) had been removed by the coated rings. Although the As(III) was assumed to be oxidized to As(V) and then adsorbed on the photocatalyst, some As(III) may adsorb directly on the photocatalyst. The tests reported herein cannot distinguish between these two mechanisms of arsenic removal.

As this test proceeded, the concentration of total arsenic in the outflow increased because the capacity of the photocatalytic adsorption medium was being used up. However, the concen-

tration of As(III) in the outflow remained constant for the entire 860 minute operation, which suggests that the oxidation rate was stable despite the adsorption of arsenic on the photocatalyst. Since the photooxidation reaction is likely occurring near the surface of the titania coating, contact between the test solution and the photoactive surface sites is critical for the reaction. Therefore, a better reactor design such as a waveguide system would likely increase the amount of arsenic removal observed in this test, which was not designed to optimize the oxidation rate.

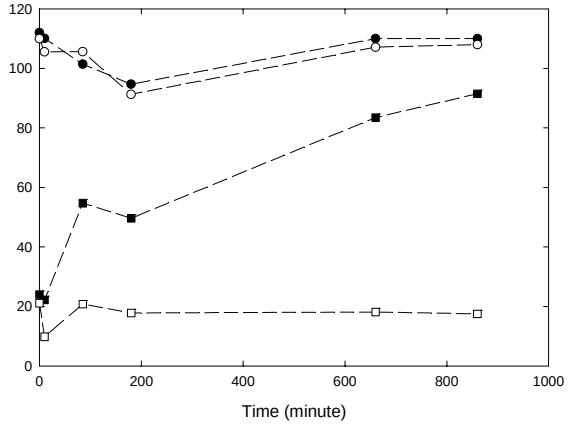

Figure 2.2. As(III) oxidation and adsorption on TiO_2-coated glass rings over 860 minutes in the presence of UV light. The y axis of this figure represents the measured concentration of arsenic in units of μg/L. Initial concentration of arsenite 100 μg/L; initial pH 7.0; (•) inflow total As, (o) inflow As(III), (■) outflow total As, (□) outflow As(III).

Effect of Dissolved Oxygen: A test solution containing 2 ppm arsenite (0.027 M) in 0.01 M $NaNO_3$ at an initial pH of 7.0 and three different DO concentrations (0.6, 1.0, and 7.0 ppm) was recirculated through the reactor at a flow rate of 10 mL/min (EBCT = 5 min). Observed rates of arsenite photooxidation were similar for DO concentrations of 1.0 and 7.0 ppm but decreased considerably at a DO concentration of 0.6 ppm. Since the molar concentration of a solution containing 1.0 ppm dissolved oxygen is 0.031 M, the results of this test suggest that DO levels may not be a significant factor in the photooxidation of As (III) as long as the molar concentration of DO is higher than the molar concentration of arsenite.

Effect of Arsenate Adsorption: In the single-pass test, arsenate was observed to adsorb on the photocatalyst. In order to determine if arsenate adsorption affected the performance of the system, 10 separate batches of the test solution employed for the dissolved oxygen study were successively recirculated through the photoreactor for about 5 hours each to determine if the photocatalyst could be deactivated over time. The photocatalyst was neither changed nor regenerated during the 10 cycles of operation.

As shown in Figure 2.3, the oxidation rates between the first and tenth batches of test solution are identical. (k_{app} for the first cycle of test solution was 2.92×10^{-3} min^{-1} and for the tenth cycle was 2.98×10^{-3} min^{-1}.) These test data indicate that the rate of arsenite photooxidation remains the same for more than 50 hours (3000 minutes) of operation without regeneration of the photocatalyst. Therefore, it appears that the adsorption of photogenerated arsenate does not affect the continued performance of the photocatalyst. In addition, Figure 2.3 shows that **1)** arsenite photooxidation is extremely slow when non-coated glass rings are used and **2)** half-order kinetics effectively models the photooxidation rate for arsenite in this test.

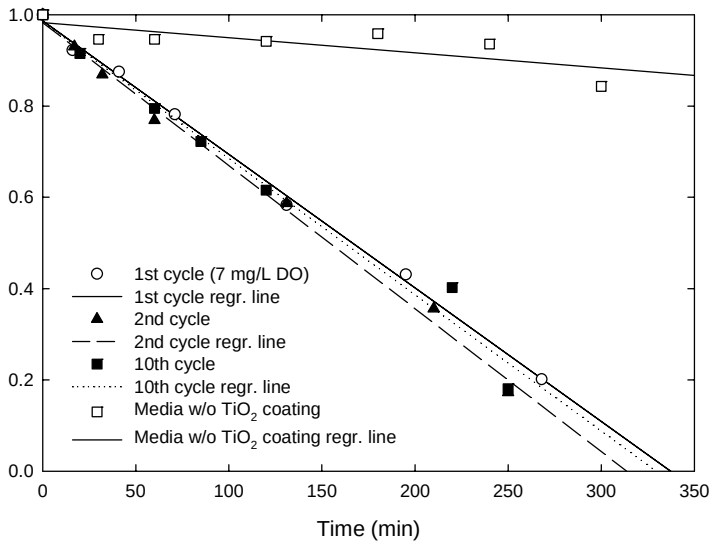

Figure 2.3. Half-order kinetics of As (III) removal for different batches of identical synthetic test solution. The y axis is $(C/C_0)^{1/2}$ for each reported test. Initial concentration of As (III) 2 ppm; initial pH 7.0; DO 7 mg/L; EBCT 5 minutes per batch.

Test with Actual Groundwater: The test to determine the effect of arsenate adsorption described above was repeated using a groundwater obtained from Danvers, IL. This water sample was treated by passing it through a 0.45 μm membrane filter to remove suspended particles. Then enough of a 1,000 ppm arsenite stock solution was added to give an As (III) concentration of 2 ppm. (The original As (III) concentration in this sample was 35 ppb, although some of this As (III) had likely oxidized to As (V) during sample collection, transport, and storage.) As observed for the laboratory solution, the rate of photooxidation with the actual groundwater sample was not significantly different between the first and tenth cycles (1.67×10^{-3} min^{-1} and 1.72×10^{-3} min^{-1}, respectively). Lowering the DO concentration to 1 ppm did not affect the observed rate of photooxidation.

However, if the rates of photooxidation in the synthetic laboratory water and the groundwater are compared, it is clear that photooxidation is slower in the groundwater. A likely explanation is that the presence of other dissolved species in the groundwater interferes with the photooxidation of As (III). Further data were obtained by measuring the rates of photooxidation of laboratory solutions of As (III) that also contained added species at concentrations similar to those present in the Danvers groundwater (Fe, Si, and organic carbon) or species that might be expected to affect the performance of the photocatalyst (phosphate and inorganic carbonate).

In these tests, the addition of any other chemical to the test solution decreased the observed rate of photooxidation, although the rates were again independent of whether the DO level was at 1.0 or 7.0 ppm. The smallest effect was observed when 0.4 ppm phosphate was present, as the rate constant decreased to 2.76×10^{-3} min^{-1}. Although it may not be present in the groundwater sample, phosphate is of interest because it binds strongly to oxides and so might be expected to affect the TiO_2 photocatalyst. Inorganic carbon (120 ppm as C) lowered the rate of photooxidation to 2.48×10^{-3} min^{-1}. Of the species known to be in the groundwater, the presence of 3 ppm iron decreased the rate to 2.37×10^{-3} min^{-1} and the presence of 8 ppm Si lowered it further to 2.15×10^{-3} min^{-1}. However, the largest effect was observed by adding enough glucose (added as a surrogate for organic carbon) to give a solution containing 12 ppm organic carbon, as

the rate decreased to 1.65 x 10^{-3} min^{-1}. This rate is almost identical to the rates observed for the groundwater sample, which contained ca. 13 ppm organic carbon. Therefore, the photocatalytic oxidation of As (III) in groundwater will be affected by the composition of the groundwater. This factor must be accounted for in designing a treatment process that includes this technology.

Conclusions

1. Glass rings coated with thin films of TiO_2 are effective for the photocatalytic oxidation of As(III) in both synthetic solutions and groundwater samples. These tests show the potential for this process to treat As(III), although further development and optimization is required.
2. The rate of photocatalytic oxidation of As (III) is unaffected by the concentration of dissolved oxygen in the water as long as enough dissolved oxygen is present. It appears that the molar concentration of dissolved oxygen should be, at a minimum, roughly equal to the molar concentration of As (III) in order to achieve the maximum rate of photooxidation. The oxidation rate is significantly slower when the dissolved oxygen concentration drops below this level.
3. The photooxidation rate does not change even after 50 hours of operation without regeneration of the photocatalyst, indicating that adsorption of arsenic on the surface of the photocatalyst does not interfere with the photocatalytic oxidation of arsenite. Therefore, this approach may provide a functional treatment process for arsenic-contaminated water.
4. As (III) photooxidation is slower in a groundwater sample than in a synthetic solution containing $NaNO_3$. The rate of oxidation is inhibited by the addition of inorganic ions including silica, iron, carbonate, and phosphate, as well as the presence of organic carbon.

Chapter 3

Field Test of Photocatalytic Oxidation Technology

Introduction

The previous laboratory study of the photocatalytic oxidation of arsenite in a groundwater sample obtained from the Danvers, IL water treatment plant indicated that the process functioned in a real-world sample. However, the actual composition of that sample was uncertain because oxidation likely occurred as oxygen was introduced to the sample during collection and then continued during storage. In addition, this sample had to be filtered before it was used in the study. Therefore, it appeared valuable to extend this study by performing a field test to verify that photocatalytic oxidation could be utilized to oxidize arsenite to arsenate in process water on site at the treatment plant. In practice, this test only involved developing a model for the kinetics of the photooxidation of arsenite to arsenate for the test system employed. No attempt was made to remove arsenic from the drinking water after photooxidation occurred.

This field test was performed at the drinking water treatment plant at Danvers, IL, a small rural community about 10 miles west of Bloomington, IL that obtains its drinking water from wells drilled into the Mahomet Aquifer. Several communities that utilize this aquifer have source waters that exceed the proposed MCL of 10 ppb for arsenic. Danvers was chosen because the facility operators in this community have a long history of cooperating with researchers at the Illinois State Water Survey (ISWS), one of whom (Thomas Holm, Ph.D.) collaborated with us on this project. As a result, these researchers have extensive knowledge about the characteristics of the water treatment processes employed at Danvers.

Whenever photocatalytic oxidation is employed in a treatment process, it is desirable to avoid loss of activity of the photocatalyst or, if it occurs, to account for it when designing the process. Such loss of activity can occur if some component(s) of the process stream and/or a product(s) of the treatment process adsorb irreversibly on the photocatalyst and block active catalytic sites. This possibility is difficult to predict in advance. An important motivation for performing this test was to determine if such a poisoning process could be shown to occur during the time frame of the test, which was roughly two days of exposure to the drinking water feed with about five hours of active photocatalytic oxidation (i.e., exposure with the light source active).

In addition, loss of photocatalytic activity can occur if some components of the process stream precipitate in the photoreactor and prevent light from reaching and activating the photocatalyst. Dissolved iron in groundwater exists primarily if not exclusively in the Fe (II) form and can be a source of such precipitation. When dissolved Fe (II) in groundwater contacts oxygen during treatment, the Fe (II) oxidizes to Fe (III), which then precipitates as some form of iron hydroxide at the neutral pH of drinking water. In order to minimize the possibility of iron precipitates affecting the test results, the water used for this test was not the groundwater being pumped into the treatment plant but rather the water that was produced after the first stage of treatment involving some aeration. Earlier tests by the ISWS indicated that the water contained only minimal levels of iron after this first treatment step.

It is possible to design photoreactors that maintain some activity even if precipitates form on the photocatalyst. One such design involves the use of waveguides that are coated with the photocatalyst. In this design, some fraction of the incident radiation is carried through the

waveguide (which needs to be essentially transparent to near-UV light for this application) and illuminates the photocatalyst from underneath whenever the radiation reflects at the surface of the waveguide [Miller et al, 1999]. A diagram of the waveguide photoreactor employed for this test is given in Figure 3.1. The reactor had been designed and fabricated for an earlier study in which light was provided by a high intensity pulsed plasma light source. Because of the high power and associated danger in operating the plasma lamp, it was not suitable for use in this field test. Although the dimensions of this reactor are not optimal for the fluorescent bulb that was utilized as a light source in this test, the reactor was suitable for testing the feasibility of photocatalytic oxidation of As (III) in real groundwater.

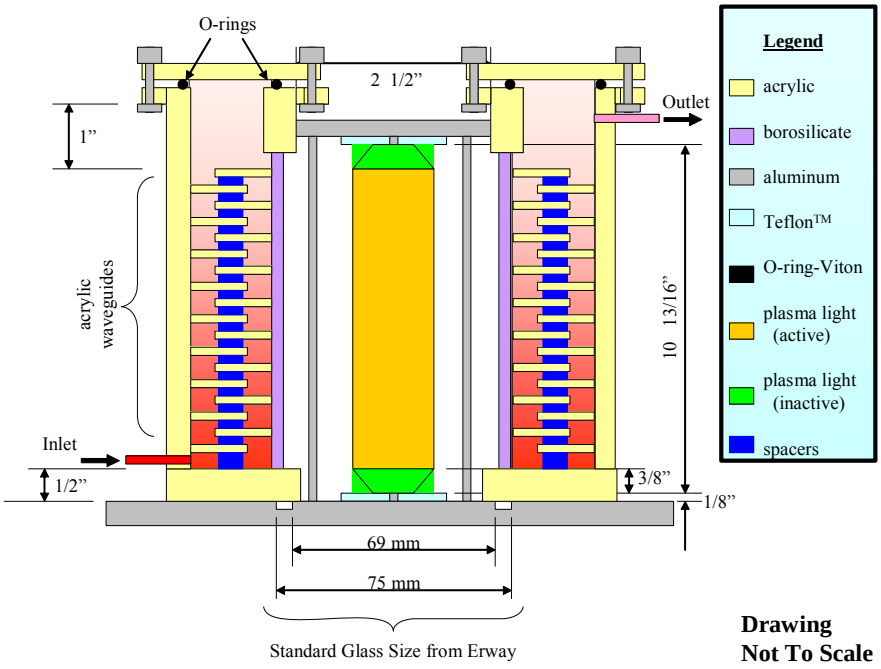

Figure 3.1. Diagram of waveguide photoreactor used to study the photocatalytic oxidation of As (III) to As (V). Diagram is not to scale, although relevant dimensions are shown.

When employing waveguide photoreactors, the coating of the photocatalyst must be thin enough to allow some of the illumination from underneath to approach the surface of the catalyst before being absorbed or else the active part of the photocatalyst will not contact the external environment. The high absorbance of TiO_2 for UV radiation requires the coatings of the photocatalyst to be only a few microns thick at most. If the coating is much thicker, then the coating must also be highly porous to allow chemical species in the external environment to contact the photoactive part of the catalyst. If these conditions are satisfied, though, deposition of a precipitate on the photocatalyst will not eliminate photoactivity in these reactors as long as the coating that forms remains porous enough to allow contact between the photocatalyst and the surrounding fluid medium.

Procedures

Waveguide Photoreactor: A fluorescent bulb with four contacts at one end (Light Sources Inc. (Orange, CT) Model GPH275T5L/4 modified to emit around 350 nm) was employed as the light source. Phosphor was applied along a 20 cm length of the bulb. (Total

length was 27.5 cm excluding the contacts.) Although this bulb was not burned in before use, it was only operated for about 6.5 hours in the on-site tests. Therefore, the irradiance produced by this bulb (estimated for a similar bulb at 5.0 mW/cm^2 some 3 mm from the surface of the bulb using an International Light Inc. (Newburyport, MA) Model IL1400A radiometer/photometer) should not have changed greatly during the course of this test.

Given the cylindrical geometry of the bulb, an annular reactor shown in Figure 3.1 was employed to collect the emitted light efficiently. The annulus held a set of disk-shaped waveguides coated with the photocatalyst. The inner wall of the photoreactor was Pyrex (69 mm ID, 27 cm height) to allow good UV transmission, whereas the outer wall and bottom were non-UV transmitting acrylic. (Most commercial acrylic does not transmit UV light effectively.) The diameter of the reactor was 14.0 cm. The reactor was designed with a removable top in order to allow stacking of the UV-transmitting waveguides. In practice, however, the reactor was operated without the top in place.

For the UV-transmitting waveguides, the photocatalyst was coated on both sides of thin disks of tanning-bed-grade methyl methacrylate with a hole cut in the center. These disks were stacked on top of each other (like a stack of vinyl records) around the central light source with thin spacers attached to one side of each disk. This configuration allows the UV light to pass into the disk, be internally reflected as it passes through the disk, and activate the photocatalytic coating at each reflection at the top or bottom of the disk. The disks were of two different sizes (both ID and OD) so that the resulting offset would allow the liquid to pass through the reactor while mixing effectively. The disks were cut out of larger sheets using a laser cutter to obtain smooth, highly polished edges to the cuts, which is essential for minimizing reflection of the incident light off the edge of the disks.

The acrylic waveguides were coated as follows: laser cut the disks from acrylic sheets, strip an adhesive coating from the disks (this coating was needed to assure correct positioning of the laser), clean the disks with ethanol, activate with an ethanolic solution of sodium hydroxide, coat with a thin layer of silica to prevent direct contact between the photocatalyst and the polymeric support, dry, coat with photocatalyst, dry. Although dip coating had been used in earlier studies to coat similar waveguides, this process is quite labor intensive. For this study, coatings were prepared by spray coating suspensions of the desired material onto the activated disks after placing the disks on a conveyor, using a commercial system available from Sono-Tek Corp. (Milton, NY). The spray coating approach worked well for this application. However, the cleaning and activation steps still required considerable labor. Commercial applications of this technology are likely to require the capability to fabricate (e.g., by extrusion) the acrylic waveguide in-house in the desired geometry followed immediately by spray coating in order to avoid the labor associated with cleaning acrylic sheets purchased from an outside source. Recent studies indicate that inclusion of an appropriate surfactant in the suspension of silica may eliminate the need for the activation step, thus simplifying this process and increasing its commercial feasibility.

The photoreactor held 48 1/8-inch thick coated disks when filled. Placement of the disks in the reactor caused the volume of liquid it held to decrease from ~ 2.6 L to ~ 1.75 L. The bulb and associated ballast were supported by the top of the reactor, with the bulb allowed to hang down into the space protected by the inner wall of the reactor. In practice, the bulb only reached about halfway down into the central core of the reactor. Therefore, the illuminated volume of the reactor was estimated to be 875 mL when calculating the empty bed contact time (EBCT).

Test System: The water treatment system at Danvers provides access to water at three stages of the treatment process: the inlet groundwater before any treatment, water after the first treatment stage (which is designed to aerate the water and remove essentially all of the dissolved iron), and the final treated water that is sent into the distribution system. Because the treated water is chlorinated, the added chlorine can oxidize any arsenite that is still present in the water. This water was not used for this test to avoid the confounding effect of an additional oxidation process occurring simultaneously with the photocatalytic oxidation process of interest. The inlet groundwater had been used for the tests discussed in the previous chapter. At the time this water sample was collected, it was noted that its visible appearance was changing even as the sample was being collected. In addition, there was enough particulate matter in this sample to require filtration before the sample was used to test the photocatalytic oxidation process. Therefore, the water used for this test was taken as a slip stream of the water after the first treatment step.

Although this treatment step was designed to oxygenate the water, it was found that DO levels in this water were quite low. As a result, initial studies performed with this water yielded limited or no photooxidation of As (III). Consequently, this water was allowed to flow into a 2-gallon bucket before use and aerated by passing air through a glass frit and a plastic aquarium aerator. This aerated water was sampled using a peristaltic pump to force water through a flow meter to control the flow rate and then into the inlet of the photoreactor. Four flow rates were tested: 75, 130, 200, and 500 mL/min. Associated EBCTs were estimated to be 11.67, 6.73, 4.38, and 1.75 minutes. Overflow from the aeration bucket and water that had passed through the reactor were sent to a drain.

Initial studies indicated that results could be affected by adsorption or desorption of arsenic from the photoreactor after previous use. To minimize these effects and attain steady-state behavior, aerated water was pumped through the photoreactor overnight (ca. 18 hours) before a test was started. Studies reported herein were performed on two different days.

Sampling Protocol: All connections were made using flexible plastic tubing, either silicone or Tygon. T connections placed before the inlet to the reactor and after the outlet allowed samples to be obtained from these locations when needed. Samples were obtained by opening the line to the desired location and using a low-flow peristaltic pump to pass the sample through a 0.4-μm syringe filter into collection bottles. One filtered sample was set aside for later analysis for total arsenic. A second sample was passed through an acetate-based anion-exchange column to remove As (V) and then set aside for later analysis for As (III). This ion exchange was performed at the Danvers site. Samples were obtained at both the inlet and the outlet of the reactor at desired times. In general, inlet and outlet samples were obtained 3 to 4 minutes apart.

For the first test, two sets of samples (i.e., samples taken from the inlet and outlet) were obtained about 15 minutes apart with no UV illumination at a flow rate of 500 mL/min, after which the UV light was activated. Some 15 minutes later, the first of 4 samples was obtained, with the remaining samples being obtained about 15 minutes apart. (This time interval corresponds to ~ 8.6 EBCTs.) The flow rate was then decreased to 200 mL/min. After 20 minutes, the first of two samples was obtained, with the second sample obtained some 20-25 minutes later (~ 4.6 EBCTs). After the second sample was obtained, the UV light was turned off and the flow rate increased to 500 mL/min. A final sample was obtained 20 minutes later.

The protocol for the second test was similar. At an initial flow rate of 130 mL/min, two samples were obtained without UV illumination about 20 minutes apart, then three were obtained with UV illumination, maintaining a 20-30 minute interval between samples (~ 3.7 EBCTs).

Once the flow rate was decreased to 75 mL/min, three samples were obtained with UV illumination, followed by two without UV illumination, at intervals of about 40 minutes (~ 3.4 EBCTs).

Analytical Procedures: Samples were taken by Dr. Holm, our collaborator on the field tests, to his laboratory at the ISWS for later analysis using graphite furnace atomic absorption (AA). The system employed was a Varian SpectrAA 220Z with Zeeman background correction, GTA 110Z graphite furnace atomizer, and PSD 100 programmable sample dispenser. All analyses were performed within one week of obtaining the samples.

For the data presented below, relative standard deviations for individual measurements were typically < 2%. Quality control (QC) during the analysis involved the use of duplicate samples, QC spikes, and QC standards. Duplicate samples were obtained by filling consecutive vials in the autosampler from the same sample bottle. The acceptance criterion for duplicate samples was 20% relative difference for concentrations over 5 times the detection limit of 0.85 ppb. For these data, only 1 of 15 duplicate samples displayed a relative percent difference > 2%. Desired spikes were added directly to samples by the instrument. Using an acceptance criterion of 80-120% recovery, all 10 spikes associated with these data sets were in compliance. QC standards were prepared from a standard arsenic concentrate (VHG Laboratories). Using an acceptance criterion of 75-125% recovery, 11 of 12 QC standards associated with these data sets were in compliance.

Data Reduction: Five kinetic models were fit to the data: zero-order, half-order, first-order, and second-order power law expressions as well as a linearized Langmuir-Hinshelwood (LH) rate expression. LH kinetic models are commonly employed to fit kinetic data obtained in heterogeneous reactions such as this one that involves a liquid reacting at the surface of a solid catalyst because an adsorption term is included in LH models. However, the equations that result from LH models generally require numerical fitting to obtain a solution. The linearized LH model was included to determine if it would provide a better fit to the data than any of the simple power law expressions.

Two approaches are commonly employed to perform kinetic studies in the laboratory. Often a sample of the reactant is placed in the reactor at a known concentration, then recycled through the reactor with subsamples drawn off at desired times and analyzed. Although this approach was employed for the studies discussed in the previous chapter, a single-pass configuration was employed for this field test. In this case, one can develop a kinetic model for the process by monitoring the change in concentration of the reactant as a function of the residence time in the reactor. This approach was employed for this study using four different flow rates. One generally maintains a constant starting concentration for the reactant in single-pass studies in the laboratory, but in this field study, the initial concentration of arsenic (i.e., the concentration at the inlet of the photoreactor) varied for each sample. Nevertheless, the equations used for data reduction in this study do not require a constant initial concentration of arsenic.

The power law expressions are all based on the following representation of the reaction:

$$dC/dt = -kC^n \qquad \text{Eq. 1}$$

where dC/dt signifies the change in concentration (C) of arsenic as As (III) with time (t), k is the rate constant for the reaction, and n is the order of the reaction, assumed to be 0, 0.5, 1, or 2 for this study. Although the rate constant k is assumed to be constant, it is a function of the irradiance or light intensity in the system and thus can vary if the irradiance changes. Because fluorescent bulbs such as that used for this study lose irradiance rather rapidly when first activated, best practice is to burn such bulbs in for at least 100 hours before use. However, it was

not possible to perform a burn-in on this bulb, which was an emergency replacement for a bulb that broke. Because this bulb was only activated for about 5 hours during this test, the irradiance is assumed to be constant. Also note that the rate constants in the different expressions that are developed cannot be compared directly because they have different units. The time t in this equation is taken as the residence time associated with a given data set.

Taking n = 0 in Eq. 1 results in the following expression:

$$C_{inlet} - C_{outlet} = kt_{res} \qquad \text{Eq. 2}$$

If this model fits the data well, a plot of $C_{inlet} - C_{outlet}$ versus t_{res} should be linear. The slope of this plot will be the rate constant for the reaction in units of ppb/min.

Taking n = 0.5 in Eq. 1 results in the following expression:

$$C_{inlet}^{1/2} - C_{outlet}^{1/2} = kt_{res}/2 \qquad \text{Eq. 3}$$

If this model fits the data well, a plot of $C_{inlet}^{1/2} - C_{outlet}^{1/2}$ versus t_{res} should be linear. The slope of this plot will be one half the rate constant for the reaction in units of $ppb^{1/2}$/min. In a case like this, the factor of 2 is usually incorporated into the rate constant.

Taking n = 1 in Eq. 1 results in the following expression:

$$-\ln (C_{outlet}/C_{inlet}) = kt_{res} \qquad \text{Eq. 4}$$

where ln represents the natural logarithm of the ratio of the outlet concentration to the inlet concentration of As (III). If this model fits the data well, a plot of $-\ln (C_{outlet}/C_{inlet})$ versus t_{res} should be linear. The slope of this plot will be the rate constant for the reaction in units of min^{-1}.

Taking n = 2 in Eq. 1 results in the following expression:

$$C_{outlet}^{-1} - C_{inlet}^{-1} = kt_{res} \qquad \text{Eq. 5}$$

If this model fits the data well, a plot of $C_{outlet}^{-1} - C_{inlet}^{-1}$ versus t_{res} should be linear. The slope of this plot will be the rate constant for the reaction in units of $ppb^{-1}min^{-1}$.

The specific LH model employed for this analysis follows:

$$dC/dt = -(kKCK_{O2}C_{O2}) / (1 + KC + K_{O2}C_{O2}) \qquad \text{Eq. 6}$$

where K represents a constant associated with the adsorption of As (III) on the photocatalyst, K_{O2} represents a constant associated with the adsorption of dissolved oxygen on the photocatalyst, and C_{O2} represents the DO concentration in the water. For the first test, the DO concentration varied between 3 and 4 ppm (~ 100 μM), whereas it varied between 5 and 6 ppm for the second test. It was shown in the previous chapter that the molar concentration of DO should be at least of the same order as the As (III) concentration for photooxidation to occur. In this case, the DO levels are considerably higher than the As (III) concentrations, which range from 6 to 22 ppb (~ 0.1-0.3 μM). Because of the large excess of DO present in these tests, the term $K_{O2}C_{O2}$ was assumed to be constant, resulting in the following reduced form of Eq. 6.

$$dC/dt = -(kKC) / (P + KC) \qquad \text{Eq. 7}$$

where P is a constant. Integration of this equation ultimately leads to the following expression:

$$-\ln (C_{outlet}/C_{inlet}) / (C_{inlet} - C_{outlet}) = kKt_{res} / P(C_{inlet} - C_{outlet}) - K / P \qquad \text{Eq. 8}$$

If this model fits the data well, a plot of $-\ln (C_{outlet}/C_{inlet}) / (C_{inlet} - C_{outlet})$ versus $t_{res} / (C_{inlet} - C_{outlet})$ should be linear. A similar form of this expression was employed by Peral and Ollis (1992). The rate constant for the reaction can be determined from the calculated values of the slope and intercept of the plot. However, the result of integrating Eq. 7 can be linearized in other ways, which will result in different values for the rate constant (Sirisuk et al, 1999). For the purposes of this project, Eq. 8 was used simply to determine how well the model fit these data.

Results and Discussion

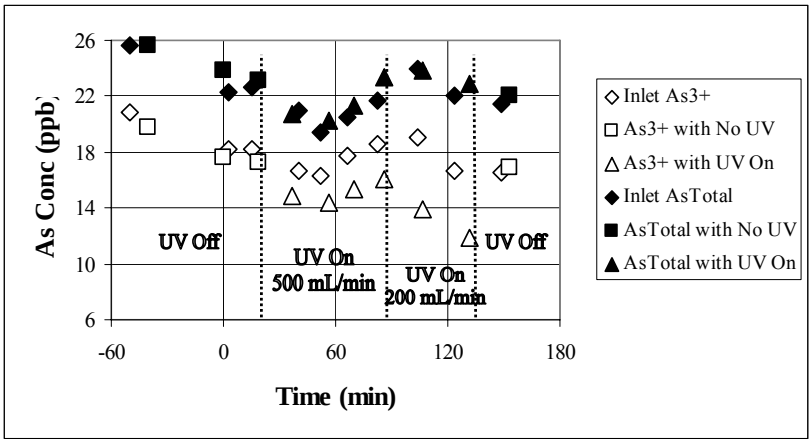

Figure 3.2. Total arsenic and As (III) concentrations at the inlet (labeled "Inlet") and outlet (labeled "No UV" or "UV On") of the photoreactor under different operating conditions during the first field test at higher flow rates. The first two data points on the left were obtained the day before the remaining data points. These points have been shifted close to the other points to make the graph legible but are shown as negative times.

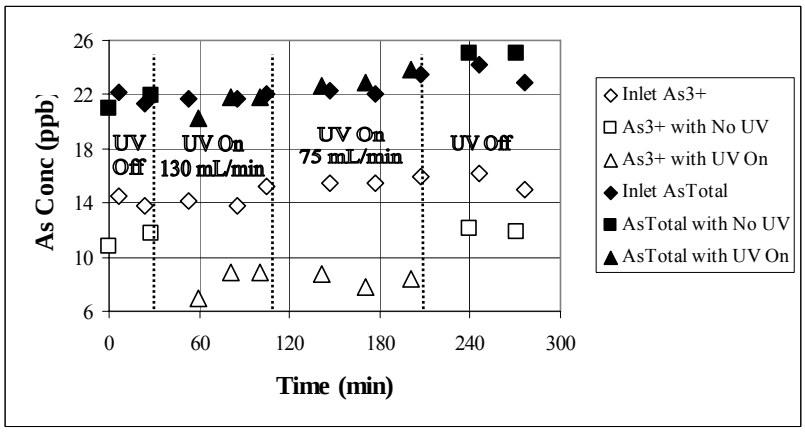

Figure 3.3. Total arsenic and As (III) concentrations at the inlet (labeled "Inlet") and outlet (labeled "No UV" or "UV On") of the photoreactor under different operating conditions during the second field test at lower flow rates.

General Performance: Figures 3.2 and 3.3 present the inlet and outlet concentrations of both total arsenic and As (III) under different operating conditions for the first and second test, respectively. Close inspection of these figures provides two observations concerning the performance of the photoreactor for treating total arsenic. **1)** Although the total arsenic being fed

to the photoreactor is predominantly in the form of As (III), a measurable amount is present as As (V). Water samples taken directly from the tap and not passed through the aeration bucket do not show the presence of As (V). Therefore, the aeration system employed for these tests caused some oxidation of As (III) before the photooxidation system. **2)** Total arsenic concentrations at both the inlet and outlet varied between 19 and 26 ppb for each test. These concentrations did not appear to be affected by passing water through the photoreactor, which indicates that the photocatalyst was saturated with adsorbed arsenic.

Further inspection of these figures offers some insight into the photocatalytic oxidation of As (III) that was the subject of this study. **1)** Photocatalytic oxidation of As (III) was observed at the field site. Under UV illumination, the concentration of As (III) at the outlet of the photo-reactor was always less than its concentration at the inlet. Because the total arsenic concentration does not change as water passes through the photoreactor, it appears that the decrease in the concentration of As (III) occurs because some of it photooxidizes to As (V). **2)** It appears that the conversion of As (III) to As (V) increases as the flow rate decreases (i.e., residence time or EBCT in the reactor increases). This behavior is expected. **3)** In the first test, the concentration of As (III) is essentially identical at the inlet and outlet of the reactor when there is no UV illumination. All of these points were obtained at a flow of 500 mL/min. During the second test, however, the concentration of As (III) was less at the outlet of the reactor even when the UV light was off. This observation indicates that a second arsenic oxidation process was occurring in the reactor even in the absence of UV light. A likely possibility is oxidation continuing from the aeration system. In this case, one would expect the amount of As (III) oxidation to increase as the flow rate decreased, as was observed. Data points with UV off at the left of Figure 3.3 were obtained at a flow rate of 130 mL/min, and data points with UV off at the right of Figure 3.3 were obtained at a flow rate of 75 mL/min.

Kinetic Analysis: The existence of two oxidation processes occurring simultaneously in the photoreactor complicates the analysis of the kinetics of As (III) oxidation. For the purposes of this test, all data obtained under UV illumination was analyzed as if only one oxidation process was occurring. In practice, a scaled-up reactor for this application would be designed based on the total oxidation of As (III) occurring in the reactor no matter how many separate oxidation processes contributed to the overall rate of oxidation.

An initial analysis was performed by averaging the input and output concentrations of As (III) for a particular set of operating conditions. These average concentrations were employed to compare the different kinetic models. A visual comparison of the resulting plots suggested that the best fit was obtained with the first-order rate expression (Eq. 4). On further consideration, though, it was felt that a better approach would be to include each data point in the plot. Results of this analysis are shown in Figures 3.4 (zero order), 3.5 (half order), 3.6 (first order), and 3.7 (second order). These plots also include a data point at (0,0) because all of these plots should pass through this point if they behave ideally. All plots include a line that shows the best least squares linear regression for the data that is forced to pass through (0,0). Results obtained with the LH model are discussed following the power law models.

It is clear visually that the zero-order model (Figure 3.4) does not fit the data well. The points appear to lie on a curve rather than a straight line, and a plot of the residuals shows definite curvature. In addition, the r^2 value of 0.742 is much lower than desired for a reasonable fit. Although the r^2 value increases to 0.855 if the regression is not forced through (0,0), this value is still lower than desired. None of the points appear to be outliers, although this supposition was not tested statistically.

Inspection of the plot for the half-order model (Figure 3.5) suggests that this model may be a better fit to the data than the zero-order model. However, the points display some curvature (as is readily apparent in a plot of the residuals), and the r^2 value of 0.803 is lower than desired for a reasonable fit, although it is slightly closer to a linear fit than the zero-order model. Although the r^2 value increases to 0.862 if the regression is not forced through (0,0), again this value is lower than desired. Visually, none of the points appear to be obvious outliers. No further analysis was performed with either the zero-order or half-order models.

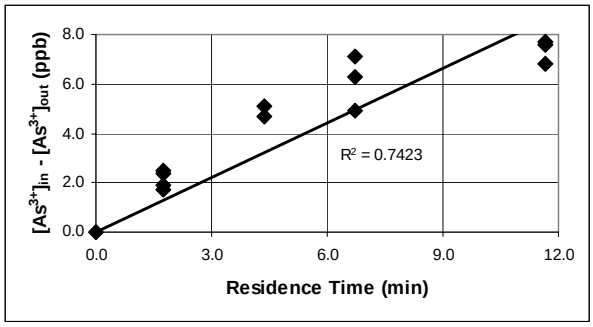

Figure 3.4. Fit of individual data points from field test to zero-order kinetics.

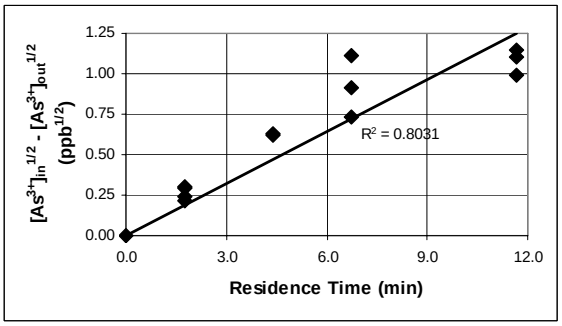

Figure 3.5. Fit of individual data points from field test to half-order kinetics.

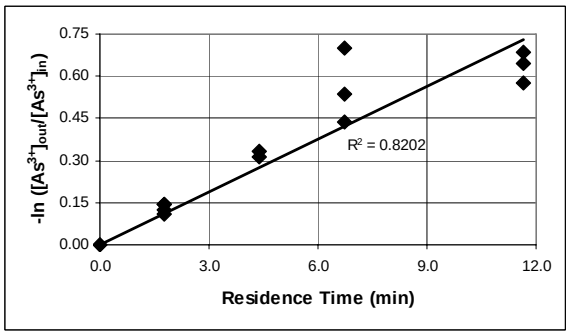

Figure 3.6. Fit of individual data points from field test to first-order kinetics.

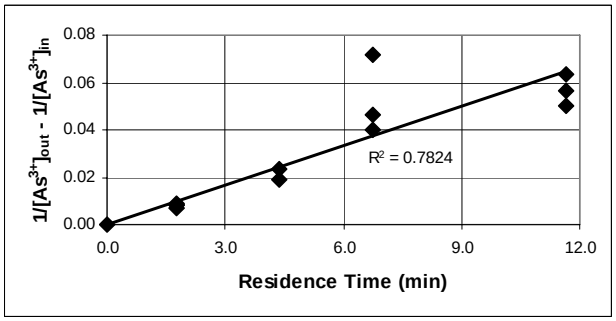

Figure 3.7. Fit of individual data points from field test to second-order kinetics.

Inspection of the plot for the first-order model (Figure 3.6) using all of the individual data points suggests that this model is no better than either the zero-order or half-order models when all data points are included. Once again, the points display some curvature that is apparent in a plot of the residuals, and the r^2 value of 0.820 is lower than desired for a reasonable fit. This value increases only slightly to 0.848 if the regression is not forced through the origin. In this case, however, there appears to be an obvious outlier. When this data set was reanalyzed excluding this point, r^2 increased to 0.922 with the fit forced to pass through (0,0) and to 0.944 otherwise. These fits provide a fair degree of linearity and suggest that the first-order model of the data could be used for design purposes. This conclusion must be tempered by noting that a statistical analysis was not performed to verify the elimination of the outlier and that the remaining points still display some curvature, which indicates that the first-order model does not fit the data completely.

Inspection of the plot for the second-order model (Figure 3.7) using all of the individual data points suggests that this model may be better than the previous three models in that this

model appears to minimize much of the curvature that was present in the other models. A plot of the residuals shows minimal curvature. Although the r^2 value of 0.782 for this model using all data points is poor, this value increases to only 0.786 when the regression is not forced through the origin, which indicates that the best fit for the original data points almost passes through the origin, as desired. As was observed with the first-order model, there appears to be an obvious outlier. When this data set was reanalyzed excluding this point, r^2 increased to 0.945 whether or not the regression was forced through the origin, which indicates that the best fit regression almost passes through the origin. Although the exclusion of the outlier was not verified statistically, the lack of curvature and the good fit through the origin with the second-order model suggest that it would be a better candidate for design purposes than the first-order model based on this data set.

Use of the second-order kinetics model would provide a more conservative design than use of the first-order model as the time required to achieve a given percent conversion is longer for a system that obeys second-order kinetics than for first-order kinetics. However, this difference does not become readily apparent until the percent conversion approaches ca. 75%. Further data would have to be obtained at Danvers at lower flow rates to confirm the appropriate order for the kinetics of the photocatalytic oxidation of As (III) in this photoreactor.

Figure 3.8 presents the LH analysis of the data. It is clear from inspection of this plot that this model provides a poor fit to the data. Removal of the most likely outlier, which is the same data point that was taken as an outlier for the first- and second-order models, increases the r^2 value to 0.760. Although removing this point provides considerable improvement in the fit, this model still would not be useful for predictive purposes. This result is somewhat surprising in that several studies have found that a similar form of the LH model accurately models photocatalytic oxidation kinetics in aqueous systems (Duffy et al, 2000 and references therein). The reason for the poor performance of this model is not known.

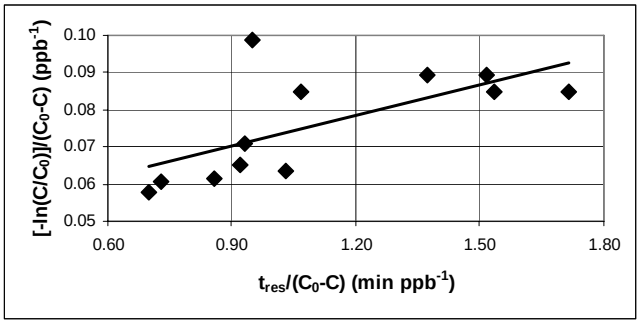

Figure 3.8. Fit of individual data points from field test to Langmuir-Hinshelwood kinetics ($r^2 = 0.444$).

Conclusions

1. The concept of using a waveguide photoreactor for water treatment, specifically the photocatalytic oxidation of As (III) to As (V), has been validated in a field test at Danvers, IL. Considerable photooxidation of As (III) was observed even though the reactor design was hardly optimal for the light source used.
2. Spray coating was used to fabricate the photocatalyst-coated waveguides that were employed for this test. It appears that spray coating offers a viable method for preparing coated waveguides that can be scaled up for industrial applications.

3. For this particular test, the best fit of the photooxidation data appeared to be to a second-order kinetics model.
4. A common Langmuir-Hinshelwood model fit the data poorly. The reason for this poor fit is not known.
5. Further development will involve designing a system that provides better coupling between the photocatalyst-coated waveguides and the light source(s).
6. The question of whether a single reactor that employs a combined photocatalyst-adsorbent (with attendant loss of efficiency for each process) or a two-stage process with separate photooxidation and adsorption stages (with attendant increase in complexity of design) performs more effectively for this process must still be addressed.

Project Conclusions and Recommendations

1. In many cases, the amount of arsenate adsorbed on activated alumina depends on the IEP of that alumina. Maximum adsorption occurs at pH values lower than the IEP. However, the value of the IEP depends on the types and concentrations of the other species present in the treatment water.
2. Adsorption of silicate and sulfate on activated alumina decreases its IEP, although the interactions with the surface appear to be different for these two species.
3. Adsorption of magnesium on activated alumina increases its IEP.
4. The use of titania-based photocatalysts is effective for the photooxidation of arsenite to arsenate whether the photocatalyst is coated on glass rings or on plastic waveguides. This process has been shown to work in the laboratory as well as in the field.
5. Effective photocatalytic oxidation of arsenite requires some dissolved oxygen to be present in the treatment water. It appears that the maximum rate of photooxidation is achieved when the molar concentration of dissolved oxygen is, at a minimum, roughly equal to the molar concentration of arsenite.
6. The photooxidation rate does not change even after 50 hours of operation without regeneration of the photocatalyst, indicating that adsorption of arsenic on the surface of the photocatalyst does not interfere with the photocatalytic oxidation of arsenite.
7. The photooxidation rate is inhibited by the presence of species such as silica, iron, carbonate, phosphate, and organic carbon in the treatment water.
8. For the field test of photocatalytic oxidation, the best fit of the photooxidation data appeared to be to a second-order kinetics model.
9. The question of whether a single reactor that employs a combined photocatalyst-adsorbent (with attendant loss of efficiency for each process) or a two-stage process with separate photooxidation and adsorption stages (with attendant increase in complexity of design) performs more effectively for this process must still be addressed.
10. In order to design effective treatment systems that utilize these technologies, the treatment water must be well-characterized. Initial on-site tests of the technology can provide useful data to assist in the design process.

References

G. Amy. Arsenic Treatability Options and Evaluation of Residuals Management Issues. Amer. Water Works Assoc. Research Found., 2000.

M.A. Anderson. Arsenic Adsorption on Amorphous Aluminum Hydroxide. Ph.D. Thesis. Johns Hopkins University, Baltimore, MD, 1974.

M. Bissen, M.M. Vieillard-Baron, A.J. Schindelin, and F.H. Frimmel. TiO_2-catalyzed photooxidation of arsenite to arsenate in aqueous samples. *Chemosphere*, **44**[4], 751-757, 2001.

H.W. Chen, M.M. Frey, D. Clifford, L.S. McNeill, and M. Edwards. Arsenic treatment considerations. *J. Amer. Water Works Assoc.*, **91**[3], 74-85, 1999.

D. Clifford. Ion exchange and inorganic adsorption. in Water Quality & Treatment: A Handbook of Community Water Supplies. American Water Works Association, Editor. McGraw-Hill Inc., New York, pp. 9.52-9.57, 1999.

S. Cornu, D. Breeze, A. Saada, and P. Baranger. The influence of pH, electrolyte type, and surface coating on arsenic (V) adsorption onto kaolinites. *Soil Sci. Soc. Amer. J.*, **67**[4], 1127-1132, 2003.

B. Dousova, V. Machovic, D. Kolousek, F. Kovanda, and V. Dornicak. Sorption of As (V) species from aqueous systems. *Water Air Soil Pollut.*, **149**[1-4], 251-267, 2003.

J.E. Duffy, M.A. Anderson, C.G. Hill, Jr., and W.A. Zeltner. Photocatalytic oxidation as a secondary treatment method following wet air oxidation. *Ind. Eng. Chem. Res.*, **39**[10], 3698-3706, 2000.

EPA. Arsenic in Drinking Water Rule Economic Analysis. U.S. Environmental Protection Agency, Washington, DC, 2000.

F.J. Frost, K. Tollestrup, G.F. Craun, R. Raucher, J. Stomp, and J. Chwirka. Evaluation of costs and benefits of a lower arsenic MCL. *J. Amer. Water Works Assoc.*, **94**[3], 71, 2002.

J.S. Geelhoed, T. Hiemstra, and W.H. vanRiemsdijk. Phosphate and sulfate adsorption on goethite: single anion and competitive adsorption. *Geochim. Cosmochim. Acta*, **61**[12], 2389-2396, 1997.

G. Ghyrie and D. Clifford. Laboratory Study on the Oxidation of Arsenic III to Arsenic V. EPA Report, Washington, DC, 2001.

S. Goldberg and C.T. Johnston. Mechanisms of arsenic adsorption on amorphous oxides evaluated using macroscopic measurements, vibrational spectroscopy, and surface complexation modeling. *J. Colloid Interface Sci.*, **234**[1], 204-216, 2001.

D.D. Hansmann and M.A. Anderson. Using electrophoresis in modeling sulfate, selenite, and phosphate adsorption onto goethite. *Environ. Sci. Technol.*, **19**, 544-551, 1985.

S.W. Hathaway and F. Rubel. Removing arsenic from drinking water. *J. Amer. Water Works Assoc.*, **79**, 61-65, 1987.

L.M. He, L.W. Zelazny, V.C. Baligar, K.D. Ritchey, and D.C. Martens. Ionic strength effects on sulfate and phosphate adsorption on gamma-alumina and kaolinite:triple-layer model. *Soil Sci. Soc. Amer. J.*, **61**[3], 784-793, 1997.

M.R. Hoffmann, S.T. Martin, W. Choi, D.W. Bahnemann. Environmental applications of semiconductor photocatalysis. *Chem. Rev.*, **95**, 69-96, 1995.

T.R. Holm. Effects of CO_3^{2-}/bicarbonate, Si, and PO_4^{3-} on arsenic sorption to HFO. *J. Amer. Water Works Assoc.*, **94**[4], 174-181, 2002.

T.R. Holm. Personal communication. 2003.

R.L. Johnson and J.H. Aldstadt. Quantitative trace-level speciation of arsenite and arsenate in drinking water by ion chromatography. *Analyst*, **127**[10], 1305-1311, 2002.

G.H. Khoe, M.T. Emett, and R.G. Robins. Photoassisted Oxidation of Species in Solution. U.S. Patent No. 5,688,378, 1997.

H. Lee and W. Choi. Photocatalytic oxidation of arsenite in TiO_2 suspensions: kinetics and mechanisms. *Environ. Sci. Technol.*, **36**[17], 3872-3878, 2002.

J. Lyklema. Adsorption of Small Ions. in Adsorption from Solution at the Solid/Liquid Interface. G.D. Parfitt and C.H. Rochester, Eds. Academic Press, New York, pp. 223-246, 1983.

X.G. Meng, S. Bang, and G.P. Korfiatis. Effects of silicate, sulfate, and carbonate on arsenic removal by ferric chloride. *Water Research*, **34**[4], 1255-1261, 2000.

L.W. Miller, M.I. Tejedor-Tejedor, and M.A. Anderson. Titanium dioxide-coated silica waveguides for the photocatalytic oxidation of formic acid in water. *Environ. Sci. Technol.*, **33**[12], 2070-2075, 1999.

J. Peral and D.F. Ollis. Heterogeneous photocatalytic oxidation of gas-phase organics for air purification: acetone, 1-butanol, butyraldehyde, formaldehyde, and *m*-xylene oxidation. *J. Catal.*, **136**, 554-565, 1992.

E. Rosenblum and D. Clifford. The equilibrium capacity of activated alumina. EPA Report No. EPA/600/2-83/107, 1984.

A. Sirisuk. Photocatalytic Oxidation of Ethylene over Thin Films of Titanium Dioxide Supported on Glass Rings. Ph.D. Thesis, University of Wisconsin – Madison, p. 195, 2003.

A. Sirisuk, C.G. Hill, Jr., and M.A. Anderson. Photocatalytic degradation of ethylene over thin films of titania supported on glass rings. *Catal. Today*, **54**, 159-164, 1999.

P.L. Smedley and D.G. Kinniburgh. A review of the source, behavior and distribution of arsenic in natural waters. *Appl. Geochem.*, **17**[5], 517-568, 2002.

R.M. Smith and E.M. Martell. Critical Stability Constants, Vol. 4. Plenum Press, New York, 1976.

J. Sun and L. Gao. Interaction forces between alumina surfaces in magnesium chloride solutions. *J. Inorg. Mater.*, **17**[2], 362-366, 2002.

L. Wang, A. Chen, and K. Fields. Arsenic removal from drinking water by ion exchange and activated alumina plants. EPA Report No. EPA/600/R-00/088, pp. 4-5, 2000.

WHO. Guidelines for drinking water quality: health criteria and other supporting information. 2nd Edition (draft). World Health Organization, Geneva, Switzerland, p. 249, 2003.

Y.T. Xiao and A.C. Lasaga. Ab-initio quantum-mechanical studies of the kinetics and mechanisms of silicate dissolution – $H^+(H_3O)^+$ catalysis. *Geochim. Cosmochim. Acta*, **58**[24], 5379-5400, 1994.

J. Zhuang and G.R. Yu. Effects of surface coatings on electrochemical properties and contaminant sorption of clay minerals. *Chemosphere*, **49**[6], 619-628, 2002.

M.E. Zorn, D.T. Tompkins, W.A. Zeltner, and M.A. Anderson. Catalytic and Photocatalytic Oxidation of Ethlyene on Titania-Based Thin-Films. *Environ. Sci. Technol.*, **34**[24], 5206-5210, 2000.